LA-UR -81-1827

TITLE: THE KRAK MODEL OF FLUID-DRIVEN FRACTURE PROPAGATION IN PERMEABLE ROCK

AUTHOR(S): BRYAN J. TRAVIS

MASTER

SUBMITTED TO: PRESENTED AT THE FIRST JOINT SPE/DOE SYMPOSIUM ON LOW PERMEABILITY GAS RESERVOIRS MAY 27 - 29, 1981, DENVER, CO.

University of California

DISCLAIMER

LOS ALAMOS SCIENTIFIC LABORATORY
Post Office Box 1663 Los Alamos, New Mexico 87545
An Affirmative Action/Equal Opportunity Employer

Form No. 836 R3
St. No. 2629

UNITED STATES
DEPARTMENT OF ENERGY

SPE

Society of Petroleum Engineers of AIME

SPE 9881

THE KRAK MODEL OF FLUID-DRIVEN FRACTURE PROPAGATION IN PERMEABLE ROCK

by Bryan J. Travis
Los Alamos National Laboratory

This paper was presented at the Society of Petroleum Engineers/Department of Energy Symposium on Low Permeability Gas Reservoirs, held in Denver, CO., May 27-29, 1981. The material is subject to correction by the author.

ABSTRACT

A model for calculating fluid-driven fracture propagation in permeable, elastic media is described. Flow in the fracture can range from small to very large Reynold's numbers. Heat and mass transport in the crack and in the surrounding porous matrix are both computed. Crack shape at each time instant is determined from Sneddon's integral and crack extension is controlled by the stress intensity integral. Flow in the crack and crack shape are fully coupled. The model has been used to show the dependence of crack propagation on material properties such as permeability and fracture toughness, on in-situ stresses and source pressure history, and on other properties.

INTRODUCTION

Control of fracture propagation is very important for the success of several in-situ technologies. For example, a goal of explosive stimulation techniques used for gas recovery from shales is to produce long fractures, thereby greatly increasing surface area available for gas drainage. In containment of underground nuclear explosions, factors causing crack growth must be understood so that such situations can be avoided. In both these technologies, fractures are driven by gases and liquids through permeable media.

Considerable effort has gone into studying isothermal hydraulic fracturing in elastic media (see, for example, Simonson et al., 1976). Abe et al. (1976) discuss the evolution of modeling of hydraulic fracturing. Much less work has been published on cracking in permeable media, particularly by compressible fluids. Pitts and Brandt (1977) considered fracture propagation in permeable media by an isothermal gas but they ignored inertial and acceleration terms in the crack flow and also considered materials with zero fracture toughness. Settari (1979) presented a model for fluid-driven fracture propagation in permeable media, but made several restricting assumptions about crack flow, crack shape and fracturing criterion. Keller and Davis (1974) developed a model for Mode I fracturing in porous, elastic media driven by hot, high-pressure steam. Davis and Travis (1977) and Travis and Davis (1980) have improved this model by adding noncondensable gases and the stress intensity factor criterion for crack extension, as well as improved treatment of the equation of state for H_2O and of the numerics in general. This last model is the subject of this paper.

KRAK MODEL.

The KRAK computer code calculates the propagation of a fluid-driven, Mode I fracture in an elastic, porous medium. Pressurized gases and/or liquids from a cylindrical source flow into a short, incipient penny-shaped crack lying in a plane normal to the cylinder axis (Figure 1). Crack extension depends on the rate of leakage of driving fluid into the porous

References and illustrations at end of paper.

medium, the mechanical properties of the medium, and the confining stress in the medium, as well as fluid pressure.

Chemical explosives generate steam and noncondensables. Also, the media of interest typically contain pore water. Introduction of hot fluids into cool, partially saturated rock will change the local saturation levels, which will result in changes in relative permeability which will affect leakage rates. It was considered important, then, to model two-phase flow in the medium. Forchheimer's relation for porous media flow

$$\vec{V}_i\ (1 + a\ Re_i\ ) = -k_i\ \nabla P_i\ /\ \mu_i \qquad (1)$$

$$Re_i = \rho_i\ L\ |\vec{V}_i|\ /\ \mu_i\ , \qquad a = 0.01/(1-\varepsilon)$$

is used in the rock since strong pressure gradients near the crack face may produce non-Darcy flow. $\vec{V}_i$ is the velocity of phase i; P_i, k_i and μ_i are the pressure, relative permeability, and viscosity of phase i, respectively. Viscosities are strongly temperature dependent; relative permeabilities depend on saturations and pressure gradients. In the crack itself, velocities can be large. Consequently, the Navier-Stokes momentum equations are needed. KRAK solves a modified form known as the Fanning equation for the velocity component V in the plane of the crack

$$\frac{\partial V}{\partial t} + V\ \frac{\partial V}{\partial r} = \frac{-1}{\rho}\ \frac{\partial P}{\partial r} - \frac{2F\ V^2}{w(r)} \qquad (2)$$

In the last term, w is the local crack width and F is the Fanning friction factor. F depends on the Reynold's number and on crack face roughness. We use an analytical fit to experimental data for F that covers the range from laminar to fully turbulent flow (Figure 2). In a crack, we assume both phases move with the same velocity.

Conservation equations for mass and energy are needed to complete the description of the flow:

$$\frac{\partial}{\partial t}\int \varepsilon\ \rho_g\ f\ d\Omega + \int (\rho_g\ \vec{V}_{gv} + \rho_{gd}\ \vec{V}_l)\cdot d\vec{A} = \int \varepsilon\ \dot{\delta}_g\ \ d\Omega \qquad (3)$$

$$\frac{\partial}{\partial t}\int \varepsilon\ \rho_{lv}\ d\Omega + \int (\rho_v\ \vec{V}_{gv} + \rho_l\ \vec{V}_l)\cdot d\vec{A} = \int \varepsilon\ \dot{\delta}_{lv}\ d\Omega \qquad (4)$$

$$\frac{\partial}{\partial t}\int \varepsilon\ E_f\ d\Omega + \int (h_{gv}\ \vec{V}_{gv} + h_l\ \vec{V}_l)\cdot d\vec{A} = \int \varepsilon\ \dot{\varepsilon}_f\ d\Omega - \int \beta(T_f - T_m)\ d\Omega \qquad (5)$$

$$\frac{\partial}{\partial t}\int (1-\varepsilon)\ E_m\ d\Omega = \int C_m\ \nabla T_m\cdot d\vec{A} + \int \beta(T_f - T_m)\ d\Omega + \int (1-\varepsilon)\ \dot{\varepsilon}_m\ d\Omega \qquad (6)$$

Separate energy equations are solved for fluid and matrix. If flow rates are high and/or the particles of the matrix are large, the fluid and the porous medium bathed by the fluid will not necessarily be in thermodynamic equilibrium.

Noncondensables are treated as perfect gases. A partially tabular equation of state is used for H_2O. In the fracture, Ω and A can vary. This allows coupling between change in crack shape and the fluid dynamics. The velocities $\vec{V}_{gv}$ and $\vec{V}_l$ are determined by equations (1) or (2).

Crack extension is determined from the stress intensity factor (Barenblatt, 1962).

$$\frac{2}{\pi\sqrt{c}}\int_{R_o}^{c}\frac{r\ Pe(r,t)}{\sqrt{c^2 - r^2}}\ dr = K_{IC} \qquad (7)$$

where K_{IC} is the critical stress intensity factor, c is crack length, R_o is the radius of the central cylindrical hole, and $Pe(r,t) = P(r,t) - \sigma(r,t)$, where P is fluid pressure in the crack and σ is confining stress. Crack width is computed from Sneddon's integral (Sneddon, 1946) for a pressurized static crack in an elastic medium.

$$w(r) = \frac{4\ (1-\nu^2)}{\pi\ Y}\int_{r}^{c}\frac{\tau d\tau}{\sqrt{\tau^2 - r^2}}\int_{R_o/\tau}^{1}\frac{x\ Pe(x\tau)\ dx}{\sqrt{1-x^2}} \qquad (8)$$

This expression should be reasonably accurate when crack velocity is much less than the elastic wave speeds of the medium. Y and ν in (8) are the Young's modulus and Poisson's ratio, respectively. Confining stress $\sigma(r,t)$ can be the earth stress or any specified distribution in space and time.

NUMERICS

The KRAK computer code solves the equations listed in the previous section using an integrated, finite difference scheme. Equation 2 is solved with a semi-implicit technique (Gentry et al. 1966). (Equation 2 is valid regardless of changes in crack volumes -- it is obtained by subtracting the mass conservation equation from the momentum conservation equation.)

Constant or time-dependent boundary conditions can be applied. Finite as well as infinite sources are allowed. Permeability can range from large values to virtually zero.

The crack tip moves through the computational mesh. A special crack tip zoning treatment provides a stable transition as the crack tip moves from zone to zone. Sensitivity to zone size in the r direction is relatively weak, but is significant in the z direction. Fine zoning is used along the crack face for accuracy. Earlier versions of the code displayed a scalloped progress of crack growth, but addition of the stress intensity integral criterion and special crack tip zoning has made crack propagation very smooth.

Coupling between crack shape, crack tip position and the fluid dynamics is complete, and is accomplished in each time step by an iterative procedure. For each time step, KRAK

(1) calculates mass and heat flow in the crack and in the matrix,
(2) uses the equation of state to determine new values of pressure, temperature, etc.,
(3) in the crack, iterates on the crack shape, crack length and the thermodynamic variables until consistency is achieved.

Sneddon's integral and Barenblatt's expression for stress intensity are evaluated analytically using piece-wise linear pressure. This analytic treatment seems necessary for stability and accuracy. Straightforward numerical evaluations produced saw-tooth crack shape profiles for occasional time steps.

MODEL VERIFICATION

We are not aware of any data that would allow all parts of the KRAK code to be tested simultaneously. Data is slowly becoming available, however. For example, an experimental program is being developed by Systems, Science and Software Corp. to generate steam-driven fractures in permeable Nevada Test Site tuff. Also, the Sandia National Laboratories has run a few air-driven fracture experiments at the Nevada Test Site. In the meantime, we have tested the various parts of the code separately.

The two-phase porous flow section of the model has been compared with analytic similarity solutions with excellent agreement. We have also compare the code with two sets of experimental data. One set consists of temperature histories recorded at various depths in a column of sand, initially dry, into which hot steam was continuously injected. Relevant material properties were measured. The code agrees quite well with this data. The other set consists of temperature histories and volumetric flow rates recorded in samples of wet, recompacted tuff into which hot, dry nitrogen was injected. Our model showed good agreement with this data. Details of these comparisons will be available in a report being prepared on the KRAK model.

One test of the fracture mechanics section of the model has been a comparison with an explosive fracturing experiment in a plexiglass block (Reference 4). Figure 3 shows the block used in one of these experiments. A cylindrical hole with grooves has been drilled into the block. Two monitoring stations are indicated. A decoupled charge of PETN was placed in the borehole and detonated. The resulting fracture propagation history was captured by a Cranz/Shardin multiple spark gap camera. Borehole pressure is shown in Figure 4. The results of the experiment are summarized in Figure 5, which indicates that the average fracture velocity was about 400 m/s, and in Figure 6, which displays the pressure history measured at station A. The pressure has two peaks, the first apparently associated with air surrounding the charge, and the second associated with the arrival of the explosive products. Gases completely filled the crack.

An attempt was made to calculate this experiment with the KRAK code. The borehole pressure of Figure 4 was used for the source. The relevant material properties of PMMA were obtained. The axisymmetric geometry that the code presently uses is not really correct for this problem; however, the width of the borehole was used for the diameter of the source. The block is thin; KRAK assumes a plate of large thickness.

Nevertheless, the calculational results are not greatly different from the measurements. The dashed line on Figure 5 indicates calculated crack length versus time and lies fairly close to the data. Crack velocity is very close to that observed. The dashed line on Figure 6 is the [illegible] lated pressure history at station A and is [illegible] gher than measured. This may be due to our idealized geometry or perhaps to reflections from the edge of the block. Figure 7 shows the pressure and crack width profiles as calculated at 200 μs. The fluid fills the crack. A second calculation was made with a reduced critical stress intensity factor K_{IC}. It is interesting that, in this case, the crack tip ran out ahead of the fluid front (Figure 8).

APPLICATIONS

One important application of the KRAK code is to determine sensitivity of fracture propagation to various physical parameters. For example, Figure 9 shows the effect of rock permeability on crack growth, all other quantities held fixed. An increase in permeability, which increases the leakage rate through the faces of a crack, sharply reduces crack velocity and will also shorten final crack length.

Another example is given in Figure 10, which shows the effect of source pressure. The large changes in crack velocity illustrate the strong positive feedback operating in the model. Higher source pressure not only is able to more easily overcome compressive stresses but also widens the crack more, greatly reducing friction losses. Much more gas is transmitted farther into the crack and more than offsets the increased leakage from the crack faces. For [illegible] conditions were 1000°C, 81.5 [illegible] steam [illegible] permeability was 2 md., porosity was [illegible] modulus was [illegible] kbars, Poisson's ratio was [illegible] stress was 25 bars, and the [illegible]

[illegible] approximate the [illegible] as a crack propagates [illegible] a high [illegible] such a [illegible] from a steam-filled [illegible] through 10 md., saturated [illegible] very permeable material (1 darcy at 80% saturation). Young's modulus and Poisson's ratio for both media were taken to be 40 kbars and 0.33, respectively. Confining stress was 25 bars. Fluid loss into the high permeability zone becomes so severe that crack growth ceases. Fracture extension into the upper layer proceeds somewhat farther when that layer's permeability is reduced to 0.1 darcy. However, the crack still stops growing. Greater source pressure can drive the fracture on through the high permeability material, as shown in Figure 12. At pressures greater than about 200 bars, the fracture will continue to extend, but at a reduced velocity.

KRAK can also handle time-dependent in-situ stress fields. In the following example, fracture propagation through a time-varying confining stress field is considered. The high pressure fluid source in this case is a large (10 m. radius) spherical cavity created by an underground nuclear explosion. When such a cavity is formed, a strong stress wave is transmitted through the surrounding rock. This transient stress field was calculated with a stress wave propagation code. The tangential stress component was used as the in-situ stress for the fracture propagation calculation. Interaction between the dynamic stress field and the growing crack is ignored, that is, the crack's effect on the local stress state is ignored. Also, transient behavior of matrix properties such as Poisson's ratio are ignored. In this example, matrix permeability was set at 5 md., porosity at 36%, Young's modulus at 30 kbars, Poisson's ratio at 0.3, grain density at 2.4 gm/cm^3, thermal conductivity at 10^5 ergs/cm·s, and specific heat at 10^7 ergs/gm°C. Initially, the rock matrix is at 30°C and 80% saturation. A small annular crack was assumed initially around the equator of the cavity. The cavity is filled with steam at 1500°C. Cavity pressure calculated for this exercise is shown in Figure 13. The stress normal to the crack plane changes with time. Figures 14 and 15 show in-situ stress profiles at 20 and 40 msecs. respectively. Crack length vs. time is plotted in Figure 16. The confining stresses do not allow crack growth until about 20 msecs. The crack begins to widen at 14 msecs. At 20 msecs., the crack begins to extend but then shuts down due to readjustments in the stress field. Finally, vigorous crack growth begins at 25 msecs. Crack width at the base of the crack becomes rather large, approaching 2 cm. Maximum crack velocity reaches 400 m/s. By 50 msec, the crack has extended about 8 m. and is slowing down. At about 55 msec, rebound occurs and the in-situ stresses increase to the point where crack growth is shut off.

These examples do not constitute an orderly, comprehensive analysis of fracture propagation in porous media. That will be the subject of a future report. These examples have been given to show the capabilities of the KRAK model. Future applications will concentrate on liquid-driven fracturing, fracture planes passing through the axis of a cylindrical source rather than normal to it, and fracturing for low Reynolds number flow.

The model has been used primarily for studies of the conditions for containment of hot, high-pressure gases generated during underground nuclear explosions. However, the model is general enough and the code flexible enough to be used for many other applications, such as explosive stimulation of gas-bearing formations.

CONCLUSION

A mathematical tool for calculating fluid-driven fracture propagation in porous media has been developed. The various parts of this model have been compared with experimental data. A variety of examples have been given to demonstrate the capabilities of the KRAK model.

NOMENCLATURE

A	area element
a	constant in Forchheimer equation
C	heat capacity
c	crack tip position
E	energy per unit volume
F	Fanning friction factor
f	gas saturation
h	enthalpy per unit volume
K_{IC}	critical stress intensity factor
k	permeability
L	local length scale, typically "average" pore size
P	pressure
Pe	effective pressure, equals $P(r,t) - \sigma(r,t)$
Re	Reynolds number
R_o	borehole radius
r	radial coordinate
T	temperature
t	time
V	velocity
w	crack half-width, function of r
Y	Young's modulus

Greek

β	heat exchange coefficient between fluid and rock
δ	mass source or sink
ε	porosity
$\tilde{\varepsilon}$	energy source or sink
μ	viscosity
ν	Poisson's ratio
ρ	density
σ	in-situ stress field
Ω	volume element

Subscripts

f	refers to total fluid
g	refers to gas component
gd	refers to gas dissolved in liquid
gv	refers to gas-vapor mixture
i	refers to phase
l	refers to liquid component
lv	refers to a liquid and its vapor
m	refers to matrix
v	refers to vapor component

REFERENCES

1. Abe, H., Mura, T., and Keer, L. M., 1976. "Growth Rate of a Penny-Shaped Crack in Hydraulic Fracturing of Rocks," J. Geophys. Res. 81, no.29.
2. Barenblatt, G. I., 1962. "The Mathematical Theory of Equilibrium Cracks." Advanced Applied Mech. 7,55
3. Davis, A. H., and Travis, B. J., 1977. "Calculation of Two-Phase Flow and Fracturing in a Porous Medium", presented at AGU Spring Meeting, Washington, D.C.
4. Fourney, W. L., and Barker, D. B., 1979. "Characteristics of a Crack Driven by Explosive Loading", Report for DOE/METC by Photomechanics Lab., Mech. Eng. Dept., Univ. of Maryland, College Park, Md.
5. Gentry, R. A., Martin, R. E., and Daly, B. J., 1966. "An Eulerian Differencing Method for Unsteady Compressible Flow Problems", J. Comp. Phys., 1, 87.

6. Keller, C. E., Davis, A. H., and Stewart, J. N., 1974. "The Calculation of Steam Flow and Hydraulic Fracturing in a Porous Medium with the KRAK Code", Los Alamos National Laboratory Report LA-5602-MS.

7. Pitts, J. H., and Brandt, H., 1977. "Gas Flow in a Permeable Earth Formation Containing a Crack", J. Applied Mech. 44, no. 4, 553.

8. Settari, A., 1979. "Simulation of the Hydraulic Fracturing Processes", Proceedings, 5th SPE Symposium on Reservoir Simulation, 187.

9. Simonson, E. R., Abou-Sayed, A. S., and Clifton, R. J., 1976. "Containment of Massive Hydraulic Fractures", presented at 51st Annual Fall Conf. of Soc. of Pet. Engrs. of AIME, New Orleans.

10. Sneddon, I. N., 1946. "The Distribution of Stress in the Neighborhood of a Crack in an Elastic Solid", Proc. Roy. Soc. A, 187, 229.

11. Travis, B. J., and Davis, A. H., 1980. "Calculation of Gas-Driven Fracture Propagation in Rocks", Proceedings, 21st U. S. Symposium on Rock Mechanics, Rolla, Mo., 356.

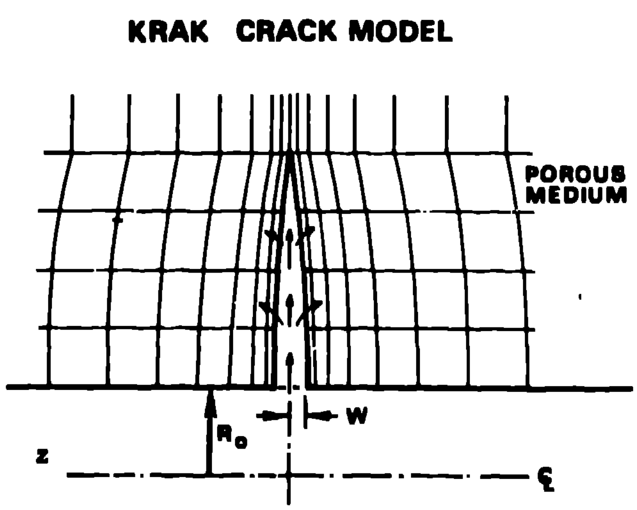

Fig. 1 KRAK model fracture geometry.

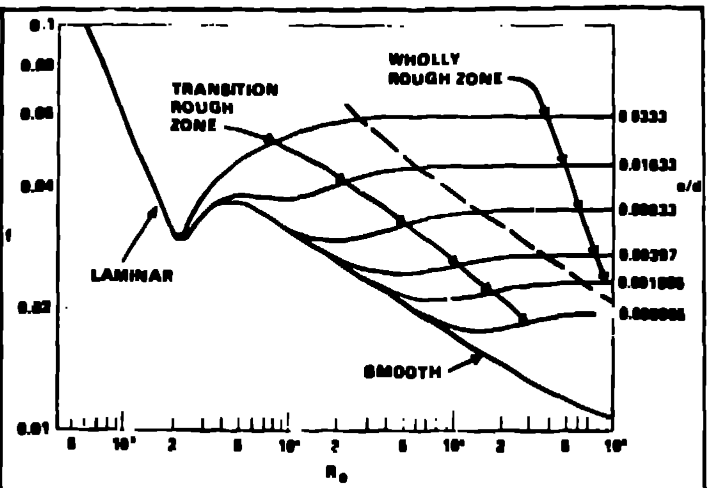

Fig. 2 Fanning friction factor.

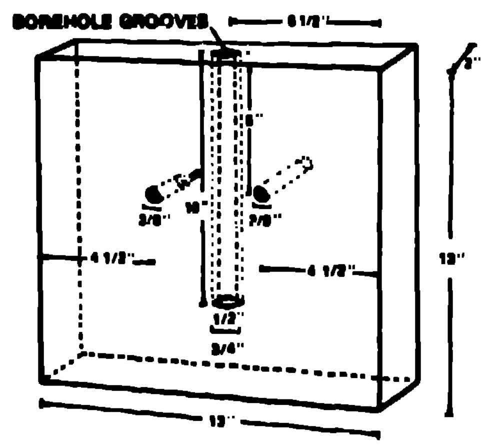

Fig. 3 Plexiglass block used for explosive fracture experiment.

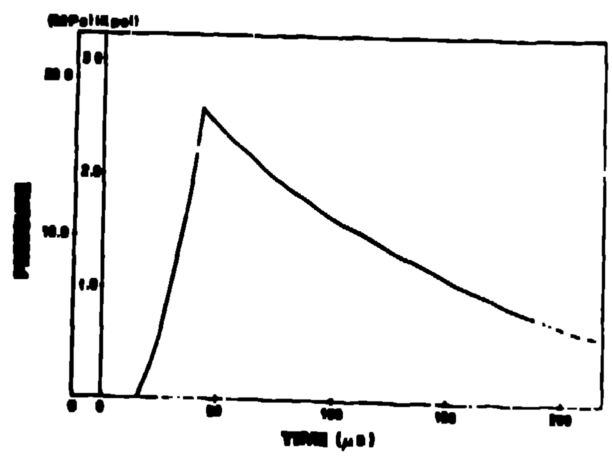

Fig. 4 Borehole pressure, used as source for calculation.

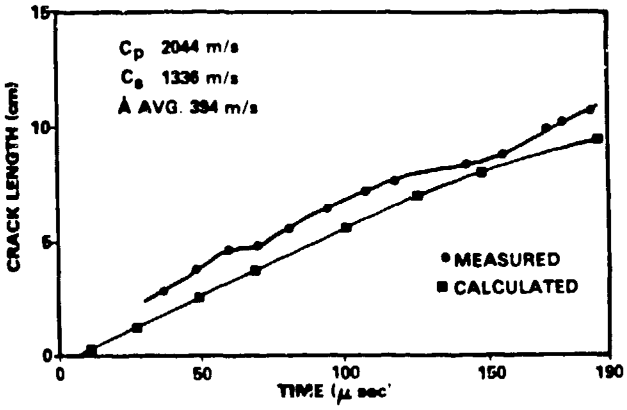

Fig. 5 Crack length vs. time.

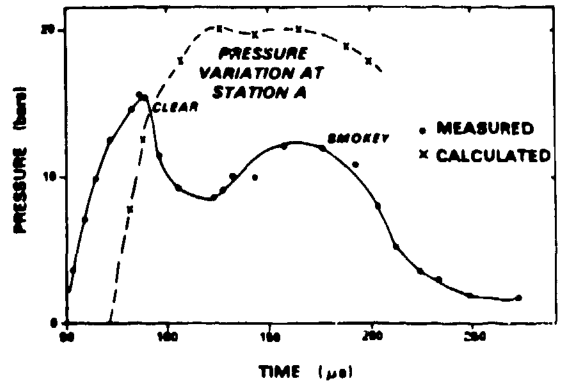

Fig. 6 Pressure at station A.

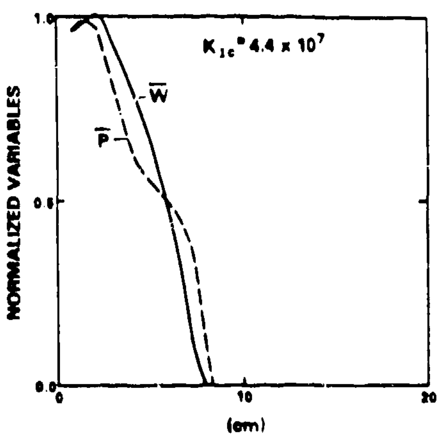

Fig. 7 Normalized pressure ($\overline{P}$) and crack width ($\overline{W}$) at 200 μsec.

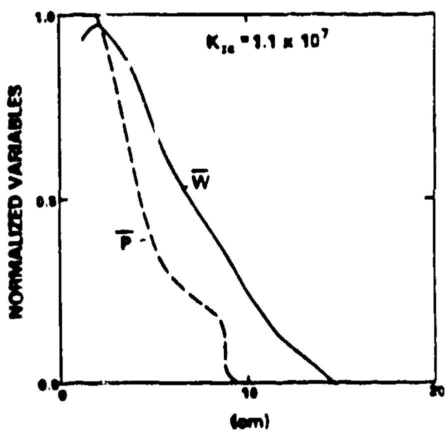

Fig. 8 Normalized pressure ($\overline{P}$) and crack width ($\overline{W}$) at 200 μsec.

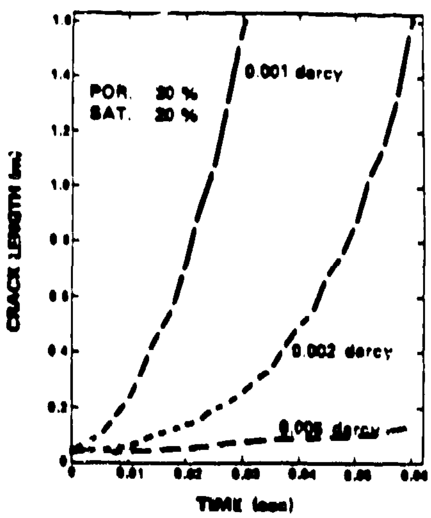

Fig. 9 Effect of permeability on crack initiation.

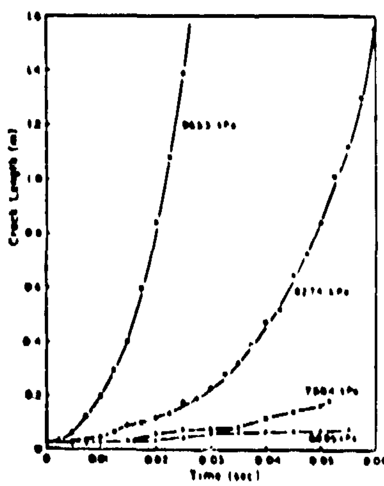

Fig. 10 Effect of source pressure on crack initiation.

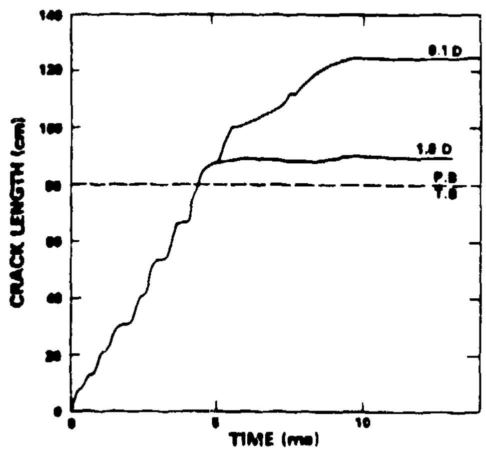

Fig. 11 Crack propagating into high permeability material.

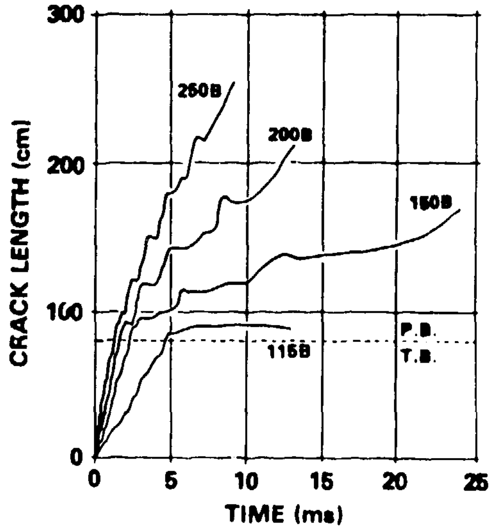

Fig. 12 Effect of source pressure on crack growth (two media case).

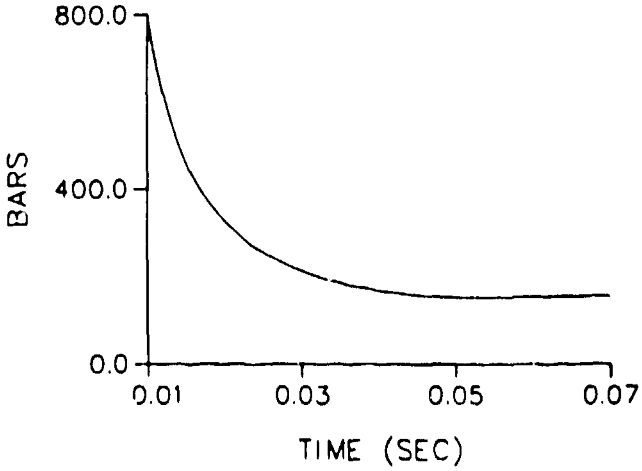

Fig. 13 Calculated cavity pressure.

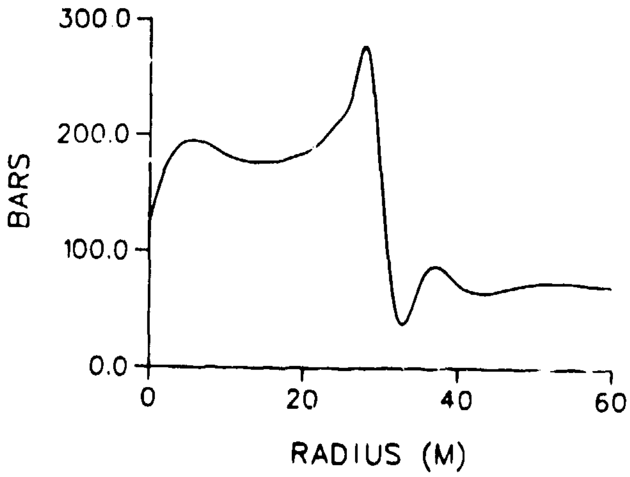

Fig. 14 Confining stress at 20 msec.

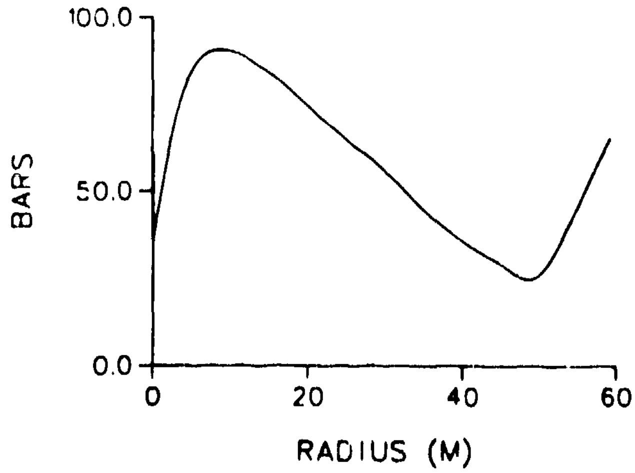

Fig. 15 Confining stress at 40 msec.

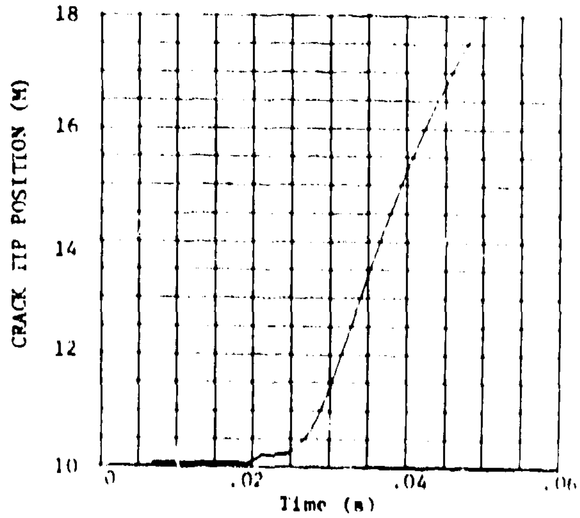

Fig. 16 Crack extension vs. time.